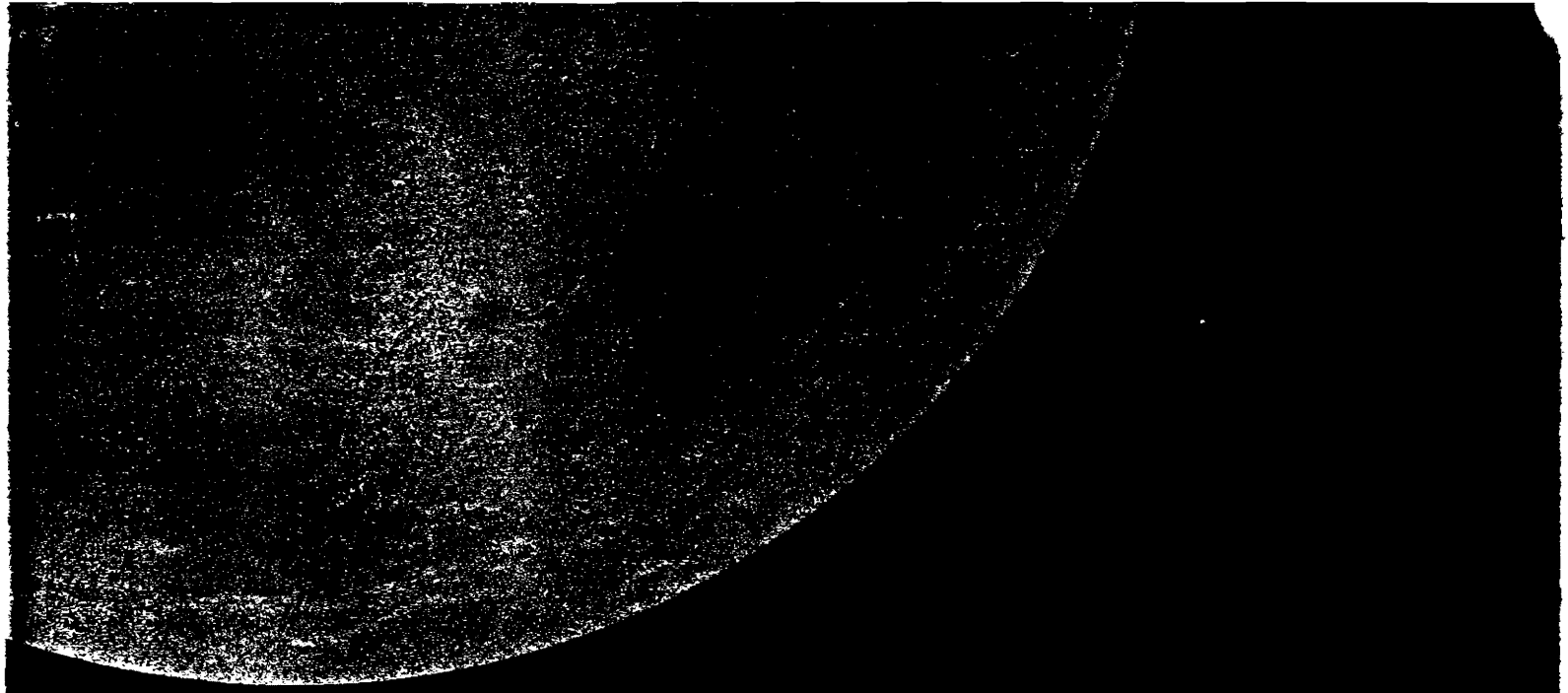

Institute of Geophysics and Planetary Physics

[illegible]

THE INTERACTION OF A SUPERNOVA REMNANT WITH INTERSTELLAR CLOUDS USING HIGH ORDER LOCAL ADAPTIVE MESH REFINEMENT METHODS

Richard I. Klein
Institute of Geophysics and Planetary Physics,
University of California, Lawrence Livermore National Laboratory
and
Department of Astronomy, University of California at Berkeley

Philip Colella
Lawrence Livermore National Laboratory
and
Department of Mechanical Engineering, University of California at Berkeley

Christopher F. McKee
Departments of Physics and Astronomy
University of California at Berkeley

To appear in "The Physics of Compressible Turbulent Mixing International Workshop", Princeton University, Ed. W. Dannevik, 1989, Springer Verlag, New York Inc., Lecture Notes Series.

THE INTERACTION OF A SUPERNOVA REMNANT WITH INTERSTELLAR CLOUDS USING HIGH ORDER LOCAL ADAPTIVE MESH REFINEMENT METHODS

Richard I. Klein
Institute of Geophysics and Planetary Physics,
University of California, Lawrence Livermore National Laboratory
and
Department of Astronomy, University of California at Berkeley
Philip Colella
Lawrence Livermore National Laboratory
and
Department of Mechanical Engineering, University of California at Berkeley
Christopher F. McKee
Departments of Physics and Astronomy
University of California at Berkeley

I. INTRODUCTION

The interaction between supernova remnants (SNR) and interstellar clouds in the galaxy is known to play a major role in determining the structure of the interstellar medium (ISM). We know that the ISM is highly inhomogeneous, consisting of both diffuse atomic clouds (T~100K) and dense molecular clouds (T~10K) surrounded by a low density warm ionized gas($T\sim10^4$K) and by a very hot coronal gas ($T\sim10^6$K). Next to radiation directly from stars, supernova explosions represent the most important form of energy injection into the ISM; they determine the velocity of interstellar clouds, accelerate cosmic rays, and can compress clouds to gravitational instability, possibly spawning a new generation of star formation.[1] The shock waves from supernova remnants can compress, accelerate, disrupt and render hydrodynamically unstable interstellar clouds, thereby ejecting mass back into the intercloud medium. Thus, while the interaction of the SNR blast wave with cloud inhomogeneities can clearly alter the appearance of the ISM, the cloud inhomogeneities can similarly have a profound effect on the structure of the SNR.

Given the importance of the interaction of the supernova shocks with clouds for understanding the structure and the dynamics of the ISM as well as the potential importance of the interaction as a means of triggering new star formation, the problem has been studied both analytically and numerically over the past decade. Even when idealized as the interaction of a strong shock with a spherically symmetric cloud embedded in a less dense intercloud medium, the problem represents an extremely complex non-linear hydrodynamic flow encompassing a rich family of shock-shock interaction phenomena. The multi-dimensional nature of the evolution of the disrupted cloud is such as to make a detailed analytic calculation intractable. The first serious attempt to follow the interaction numerically was made by Woodward[2], who

used a combined Eulerian-Lagrangian approach to follow the interaction of the shock from a spiral density wave with a galactic cloud. These results showed the start of both Rayleigh-Taylor and Kelvin Helmholtz type instabilities; however, the calculation was not carried out far enough to ascertain the final fate of the cloud. A subsequent attempt to investigate this problem by Nittman et al.[3] used a flux-corrected transport approach and was very unresolved. Recently, Tenorio-Tagle and Rozyczka[4] attempted to follow the evolution with a second order accurate hydrodynamic scheme, but again the calculation was under-resolved and clearly showed the effects of strong numerical diffusion at the interface of the cloud boundary and the intercloud medium. This made it impossible to disentangle the mixing of cloud-intercloud matter due to physical instabilities from mixing due to numerical effects. All of the previous work on this important problem leave unanswered several questions of key importance: What is the ultimate fate of clouds that have been impacted by SNR shocks? What is the total momentum delivered to the cloud? How much mass is lost from the cloud? To what extent is the cloud disrupted? How do the results scale with cloud density, shock Mach number and cloud size? Is the cloud driven to gravitational instability or is the cloud destroyed? What is the effect of the interstellar magnetic field on the evolution? What are the observable consequences of the interaction?

As we shall see, highly complex shock-shock interactions play a major role in determining the morphology of the cloud. Instabilities and shear flow motions are crucial to track accurately. These physical phenomena place an enormous constraint on the capabilities of most conventional numerical methods for solution in 2-D. Even high order accurate approaches such as PPM[5] with fixed Eulerian grids would require at least 10^6 grid points to follow the evolution accurately enough to answer the questions posed above. Clearly, one has a great need to evolve solutions in 2-D with a great enough accuracy to deal with physical constraints and at the same time do so <u>economically</u> in both storage and time.

II. METHODOLOGY

To address these difficulties, we have used the local adaptive mesh refinement techniques with second order Godonov methods developed by Berger and Colella.[6] This first important problem will be the forerunner of a broad-based program we are developing to use adaptive mesh refinement to study astrophysical gas dynamics. We employ a second order finite difference solution of the Euler equations on a square grid in a cylindrically symmetric geometry. The numerical integration of the Euler equations is accomplished using an operator split version of a second order Godunov method (Van Leer,[7] Colella and Woodward[8]). The Godunov method conserves mass, momentum and total energy. We use a γ law equation-of-state, with the cloud and intercloud medium potentially having differing γ. The resulting method is second order accurate in space and time, and captures shocks and other discontinuities with minimal numerical overshoot and dissipation.

The fluid interface is modeled using the SLIC[9] algorithm. In this approach the fraction f of the cell occupied by the cloud is determined for each grid cell through which the cloud interface passes. At the end

of every timestep a simple picture of the interface consisting entirely of vertical and horizontal line segments is reconstructed from the volume fraction information. This picture is then used to determine how much of each fluid is convected out of the cell into adjacent cells at this time step and an update of the partial volumes associated with each cell is obtained. A possible difficulty of this approach is that in a region of expansion or compression, both fluids in a multi-fluid cell will be expanded or compressed equally, regardless of the difference in compressibility between them. To correct this difficulty, we use a scheme in which the equations of motion are rewritten to include extra evolution equations for the volume fraction, total energy of each fluid, and mass density of each fluid in multi-fluid cells. This takes into account the fraction of each fluid component in the cell in such a way as to ensure the correct relative expansion or compression of each fluid component.

From the point of view of being able to resolve detailed complex physical structures with reasonable amounts of supercomputer time and memory, the most important feature of our code is that it employs a dynamic regriddng strategy known as Adaptive Mesh Refinement (AMR)[6] to dynamically refine the solution in regions of interest or excessive error. This is effected by placing a finer grid over the region in question with the grid spacing reduced by some even factor (typically 4). The boundary of the refined grid is always chosen to coincide with cell edges of the coarser grid. Multiple levels of grid refinement are possible with the maximum number of nested grids supplied as a parameter in the calculation. Typically our calculations employ two nested grids over the initial coarse (level 1) grids. In our present work, we determine those regions which require refinement by estimating the local truncation error in the density and refining those regions where the error is greater than some initially specified amount. In addition, we require the maximum level of refinement in the neighborhood of all cells containing cloud material. Special care is taken to ensure the correct fluxes across boundaries between and fine grids. This dynamic adaptive gridding approach is a crucial factor in our ability to economically resolve important features in the cloud shock interaction.

An important feature of our method is that the mesh is locally refined in space-time by $r=\Delta X_{l-1}/\Delta X_l$ on all grids, where ΔX_l is the grid spacing on level l. This implies that the explicit difference scheme remains stable on all grids. In our approach, refined regions appear and disappear in time as they are needed. Given that high resolution second order Godunov schemes are necessary to resolve key features of the interaction, but may still be expensive, AMR concentrates the computational effort in regions where it is most needed without sacrificing accuracy anywhere else. This is in contrast to moving grid approaches. Here one is pulling grid-lines into one region at the expense of sacrificing accuracy elsewhere, giving a fixed cost for the most accurate solution. Grid moving methods have inherent difficulties. There are problems maintaining smooth grids; regularity terms and penalty functions for grid regularization can be complicated and expensive, and one must initially guess at the adequate number of grid points necessary to resolve features that may appear. On contrast, AMR obtains a fixed accuracy at minimum cost. Grid points are added or removed as is necessary to maintain a desired accuracy.

III. CLOUD SIZE SCALES

As the SNR expands through the ISM, it drives a shock into any cloud it encounters. Assuming that these are strong shocks, the pressure behind the blast wave and the pressure behind the transmitted cloud shock are comparable, and one finds that (McKee and Cowie)[10]

$$v_s \approx (\rho_i/\rho_c)^{1/2}\, v_b \ , \tag{1}$$

where v_s and v_b are the cloud shock and blast wave velocities and ρ_c and ρ_i the cloud and intercloud densities, respectively. Following McKee[1], we define characteristic timescales for the cloud-shock interaction. Let $\chi \equiv \rho_c/\rho_i$ be the density and assume that $\chi >> 1$. Assume that the cloud is a sphere with radius a at a distance R from the supernova explosion. The blast wave in the Sedov-Taylor phase will expand as $R_b \propto t^{2/5}$. We can define the cloud crushing time,

$$t_{cc} \equiv \frac{a}{v_s} = \frac{\chi^{1/2}\, a}{v_b} \tag{2}$$

the intercloud crossing time,

$$t_{ic} \equiv \frac{2a}{v_b} \tag{3}$$

and the age of the SNR,

$$t \equiv \frac{dR_b}{dt} = \frac{2}{5}\frac{R_b}{v_b} \tag{4}$$

The cloud is destroyed by thermal evaporation or by hydrodynamic instabilities in a time of order $t_d \sim \chi^{1/2}\, t_{cc}$, which is comparable to the time for drag forces to bring the cloud to rest in the intercloud medium.

In this paper, we will consider only clouds that can be characterized as "small", so that the SNR does not evolve significantly during the time for the cloud to be crushed: and we find that

$$t > t_{cc} \Rightarrow a < \frac{0.4R}{\chi^{1/2}} \tag{5}$$

Indeed, we shall focus on the case in which the cloud is "very small", so that $t >> t_d$, and $a << 0.4R/\chi$. In either case, we have $a << R$ so that the blast wave may be treated as a planar shock. In the opposite limit of a shock interaction with a large cloud the SNR blast wave will undergo substantial weakening over the time it takes to cross the cloud. We expect substantial disruption for the small clouds, but only impulsive effects for large clouds.

IV. RESULTS

Since there are no intrinsic scales in the problem, it is parameterized by the Mach number of the SNR blast wave M and the density ratio χ. Our calculations assumed 2-D axisymmetry for an inviscid fluid with no magnetic field. Two cases were considered for the cloud: $\gamma=1.1$ and $\gamma = 5/3$. The intercloud gas was assumed to have $\gamma = 5/3$. Several calculations have been made for Mach numbers in the range $10\text{-}10^3$ and density ratios $10\text{-}10^2$.

It is useful to follow the morphological evolution of the cloud through several cloud crushing times to obtain a sense of the different stages of development. We present the time-development of the isodensity contours of the cloud for the case γ (cloud) = γ (intercloud) = 5/3, χ=10, M=10. At $t=0.84t_{cc}$ (Fig. 1), the transmitted shock is compressing the cloud from the front, secondary shocks have enveloped the sides of the cloud as the blast wave passes over the cloud, and a reflected bow shock moves upstream into the intercloud medium. The reflected shock becomes a standing bow shock and eventually a weak acoustic wave carrying away a small amount of energy from the supernova shock (Spitzer, 1982). At $t=1.05t_{cc}$ (Fig. 2) the blast wave behind the cloud reflects off the axis giving rise to a Mach reflected shock back into the cloud. After $t=1.26t_{cc}$ (Fig. 3), behind the cloud, a double Mach reflection with the appearance of two triple point interactions occurs. This classic oblique shock interaction[12,13] shows evidence of a strong supersonic vortex ring far behind the cloud. The vortex ring may have interesting observational consequences for SNR (see below), but plays no role in the continued dynamical evolution of the cloud. The reflected shock and the transmitted shock undergo a strong interaction at $t=1.68t_{cc}$ (Fig. 4) resulting in a initial flattening of the cloud. We also note the beginning of a strong shear flow. The vorticity is efficiently produced by strong components of $\nabla\rho X\nabla P$ at the interface. Substantial flattening of the cloud is observed at $t=2.1t_{cc}$ from the strong shocks which have squeezed it like a vise. The pressure maximum on the nose of the cloud exceeds the pressure minimum on the sides and the cloud begins to expand laterally[3] (Fig. 5). We note the growth of Richtmyer-Meshkov[13] instabilities on the cloud nose which grow more slowly than the classic Rayleigh Taylor modes. At $t=2.5t_{cc}$, we see evidence of Kelvin Helmholtz instabilities, on the sides of the cloud; weak shocks still residing in the cloud interior dissipate their energy (Fig. 6). At $3.78t_{cc}$ a prominent shear layer exists through the cloud. This shear is caused by a combination of the effects of the downstream reflected shock keeping high pressure in the center of the cloud relative to the sides, the effects of the cloud moving through the ICM, and the development of Kelvin-Helmholtz instabilities. The shear produces copious vortex rings along the shear flow layer and leads to substantial Kelvin Helmholtz instabilities which break up the arms (Fig. 7). The cloud consists of a distorted unstable axially flattened core component and a severely disrupted halo of cloud material. Over 70% of the original cloud mass is in small fragments which, in the absence of cooling, should merge with the intercloud medium. The unstable break up is dominated by large scale differential shear. Finally, at $t=9.7t_{cc}$ the cloud is essentially destroyed. The cloud consists of multitudes of small fragments distributed along a halo structure with an aspect ratio of about 6, with no evidence of a core component (Fig. 8).

Let us consider the characterization of the evolution of the interstellar cloud in more detail. In Table 1, we display the results of adiabatic calculations for three models where $\gamma=1.67$ in both the cloud and ICM for all cases. The calculations are done for two models of M=10 and 100 for density contrast $\chi=10$ and one model M=100 and density contrast 100. The first entry in the table is the time normalized to the intercloud crossing time. The second entry gives the time normalized to the cloud crushing time and the drag time, $t_d = \chi^{1/2} t_{cc}$. The next column is the sound speed behind the cloud shock normalized to the blast wave velocity. It can be shown that the initial cloud shock can accelerate the gas up to 3/4 v_s for non-radiative shocks, so the next entry is a measure of the fraction of the velocity currently in the cloud to its maximum possible velocity; in the frame of the shocked intercloud gas, this is a measure of cloud deceleration. The next column is a characterization of the cloud's aspect ratio in the radial and axial direction weighted by its half mass distribution. Here $r_{1/2}$ is the radial half-mass distance and $Z_{1/2}$ is the axial half-mass distance. The last column gives the radial $\dot{r}_{1/2}$ and axial $\dot{Z}_{1/2}$ dispersion velocities of the cloud to quantify the amount of stretching the cloud undergoes as it is subjected to shearing. These velocities are computed by using the half mass distance distributions at the two final times in the calculation.

Several conclusions can be drawn from these results. Comparing the results at the same normalized "final" time $t=4.2t_{cc}$ for clouds of the same density $\chi=10$, but subjected to blast waves of different Mach number 10 and 100, we note that both clouds have decelerated to about 0.15 of their initial velocities. Thus, these clouds have almost stopped, leading to a small pressure differential between the front of the cloud surface and the sides so that there is little force driving further radial expansion; hence the clouds have a radial dispersion velocity $\dot{r}_{1/2} \approx 0$. The strong shear flow in the cloud is still dominant, however, and both clouds are supersonically shearing apart at about the same axial dispersion velocity $\dot{Z}_{1/2}$ of 3 times the cloud velocities. The physical extent of the stretching in both the radial and axial direction

$$\frac{r_{1/2}(t)}{r_{1/2}(0)}, \frac{Z_{1/2}(t)}{Z_{1/2}(0)}$$

when compared to the characteristics cloud size initially is essentially the same. The remarkable agreement of these features of the clouds leads one to suspect that the cloud evolution may scale similarly with the Mach number of the SNR shock. In fact, if we look at the isodensity contours of both clouds at $t=4.2t_{cc}$, we clearly see the evolution is similar (Fig. 9a,b). This Mach scaling can be clearly seen if we scale the time, velocity and pressure as $t' = t/M$, $v' = vM$ and $P' = PM^2$. Substituting these scaled quantities into the Euler equations, we find that Euler equations are invariant under this transformation. Thus, we find that for fixed γ and density, the morphological evolution is a function of t/t_{cc} only in the limit of large M. At $t=3.78t_{cc}$ (Fig. 7), the cloud is experiencing a large drag due to the lateral increase in its surface area associated with the highly flattened core component. This results in the large deceleration as the cloud is slowed to .16 of its maximum velocity. At the final time $t=9.7t_{cc}$ in the calculation, the cloud has

essentially been destroyed (Fig. 8). We note that the cloud has decelerated to 0.07 of its original velocity and has essentially stopped expanding axially as well as radially. The final fate of this cloud consists of a quasi-static halo of fragments of which 50% of the mass resides in an axially elongated distribution stretched out 5-6 times its initial shape, and the rest of the mass resides in a multitude of fragments much less dispersed. If we consider the case with χ=100, we note that the cloud has a large aspect ratio and appears to be substantially more radially compressed than the lower density cloud. This can be understood by considering that the shock passes over the cloud far more rapidly than the cloud shape can change, and a quasi-steady flow is established around the cloud with a pressure maximum at the front of the cloud and a pressure minimum on the sides. The gas passes through a sonic point point as it flows past the cloud. A rarefaction wave moves into the shocked cloud (Nittmann and Falle[3]) producing velocities of the order of the sound speed so that the cloud expands laterally at the sound speed. It is easily shown that the sound speed

$$c \propto \left(\frac{\rho_i}{\rho_c}\right)^{1/2} v_b \ ,$$

so for the higher densities the cloud expands much more slowly and appears radially compressed. These clouds have less drag and so experience less deceleration than the less dense clouds. We also note that at $t=4.3t_{cc}$, the cloud is still axially supersonically shearing. As remarked above, the destruction time for the cloud t_d is comparible to the drag time $\frac{a\chi}{v_b}$ and our simulation confirms that the small clouds experience substantial ablation after a few drag times.

We have performed calculations for several similar models for γ=1.1 in the cloud.[15] This softer equation-of-state is more representative of clouds that are radiative, although it should be pointed out that truly radiative clouds can get rid of their stored energy efficiently, and we would expect substantially more shock compression than the models considered here. We note that these "radiative" clouds move substantially more rapidly than their γ=1.67 counterparts. These clouds are significantly more radially compressed, and thus experience far less drag than the γ=1.67 clouds. This can again be understood by consideration of the sound speed in these clouds. We find that the scaling of sound speed c with γ is such that $c(\gamma=1.1) << c(\gamma=5/3)$, so that these "radiative" clouds expand laterally more slowly. We note that the high density "radiative" cloud is still experiencing large supersonic axial shearing. As with the previous models Mach scaling appears to be established.

An outcome of these calculations that may be potentially very important for observations of SNR is the discovery of the copious production of vortex rings distributed along the strong shear flow layer (Fig. 10). In this graph of iso-vortex contours at $t=5.0t_{cc}$ we see formation of many points of high vorticity. Approximating the rotation of these vortices by rigid body rotation, we can relate the vorticity ω in an individual vortex ring to the pressure differential across the vortex ΔP, and we find that

$\omega = (8\Delta P/\rho)^{1/2}\ 1/r$. This appears to be an excellent approximation when compared to our detailed calculations. Recent high resolution radio observations of the Cas A SNR(Tuffs[16]) have revealed several hundred intense compact radio emission peaks distributed throughout the remnant. We have demonstrated that strong shear flows associated with shock cloud interactions result in the production of many supersonic vortex rings. These vortex rings can be expected to wind up ambient magnetic fields present in the interstellar clouds until equipartition between the energy in the field and the vortex is achieved. It is quite possible that the resulting intense wound up magnetic field could account for the synchrotron emission of electrons, thus explaining the observations in Cas A. Chevalier[17] (1976) postulated the presence of turbulent vortices, acting as magnetic scattering centers in SNR's to explain particle acceleration by a second-order Fermi mechanism. We conjecture that the radio hot spots may indeed be indirect observational evidence of the presence of vortex rings produced behind the shocked clouds.

V. CONCLUSIONS

We have performed, for the first time, second order accurate high resolution local adaptive mesh refinement calculations of the interaction of a supernova shock with interstellar clouds. These extremely powerful hydrodynamic techniques have enabled us to calculate exceedingly complex flows much more rapidly and much more accurately and much further in time than previous work with standard fixed grid hydrodynamics. We have followed the evolution of interstellar clouds well into the regime of fragmentation. Our calculations have demonstrated high accuracy with 80,000 grid cells in the cloud that would only be achievable with fixed grid high order accurate hydrodynamic schemes with >1,000,000 grid cells. We find:

1) Small interstellar clouds are efficiently destroyed in a few cloud drag times by combined Rayleigh-Taylor and Kelvin Helmholtz instabilities dominated by large scale shear flow. Clouds that have the same density but are enveloped by strong shocks of differing Mach number exhibit scaling behavior in their morphological evolution.
2) Small clouds are highly fragmented. Cloud fragments will most likely feed their mass back into the ISM by thermal conduction.
3) Small clouds fragment to such an extent that it is unlikely that fragments large enough to become gravitationally unstable and form stars will survive. This conclusion is based on the present adiabatic calculations and may not apply to radiative clouds or clouds which are not "small".
4) Clouds evolve toward a elongated structures with aspect ratios of five to six consisting of multitudes of fragments.
5) Our calculations indicate the copious production of supersonic vortex rings. Those rings with large aspect ratio may be subject to non-axisymmetric instabilities and break up into yet smaller vortex structures.[18] "Fat" rings, with small aspect ratio, are likely to remain intact. These vortex rings may be effective in winding up the ambient magnetic field in clouds, increasing the magnetic field strength and enhancing the synchrotron emission of cosmic ray electrons. This could explain the recent observations of numerous compact radio hot spots in Cas A.

In the future, we will be using adaptive mesh refinement hydrodynamic techniques to investigate a broad range of astrophysical gas dynamical phenomena.

ACKNOWLEDGEMENTS:

The calculations presented in this paper were performed on the XMP416 at the Lawrence Livermore National Laboratory. This work was performed under the Auspices of the U.S. DOE by LLNL under Contract W-7405-Eng-48, and was also performed in part under the auspices of a special NASA astrophysics theory program which supports a joint Center for Star Formation studies at NASA Ames Research Center, University of California, Berkeley, and University of California, Santa Cruz.

Table 1

	t/t_{ic}	t/t_{cc} t/t_{drag}	c/v_b	$\frac{4}{3}(v_c/v_b)$	$r_{1/2}(t)/r_{1/2}(0)$ $Z_{1/2}(t)/Z_{1/2}(0)$	$\dot{r}_{1/2}/v_b$ $\dot{Z}_{1/2}/v_b$
$\chi=10$ / $M=10$	6.7	4.2 1.3	0.18	0.16	1.8 3.2	~0.0 0.35
	15.3	9.66 3.0		0.074	2.38 5.69	~0.0 ≤0.045
$M=100$	6.7	4.2 1.3	0.18	0.14	2.0 2.6	~0.0 0.32
$\chi=100$ / $M=100$	21.3	4.3 0.43	.056	0.25	3.7 8.4	~0.0 0.42

BIBLIOGRAPHY

1. McKee, C. F., 1988, IAU Coll.101, Supernova Remnants and the Interstellar Medium, Ed. R. S. Roger and I. L. Landecker, Comb. Univ. President, 205.

5

2. Woodward, P., 1976, Ap.J., 207, 464.

3. Nittman, J., Falle, S., and Gaskell, P., 1982, N.N.R.A.S., 201, 833.

4. Tenorio-Tagle, G., and Rozyczka, M., 1986, Astron. Astrophys., 155, 120.

5. Woodward, P. and Colella, P., 1984, J. Comp. Phys., 54, 115.

6. Berger, M. J., and Colella, P., 1989, to appear in J. Comp. Phys.

7. Van Leer, B., 1979, J. Comp. Phys. 32, 101.

8. Colella, P. and Woodward, P., 1984, J. Comp. Phys. 54, 174.

9. Noh, W. F. and Woodward, P., 1976, UCRL Preprint No. 77651.

10. McKee, C. F. and Cowie, L. L., 1975, Ap.J., 195, 715.

11. Spitzer, L., 1982, Ap.J., 262, 315.

12. Hornung, H., 1986, Ann. Rev. Fluid Mech., 18, 33.

13. Glaz, H. M., Colella, P., Glass, I.I., Deschambault, R. L., 1985, Proc. Ray. Soc. Lond. A 398, 117.

14. Richtmyer, R.D., 1960, Comm. Pur. Appl. Math., 13, 297.

15. Klein, R. I., Colella, P. and McKee, C. F., 1989, Ap. J. in preparation.

16. Tuff, R. J., 1986, M.N.R.A.S., 219, 13.

17. Chevalier, R. A., 1976, Ap.J., 207, 450.

18. Saffman P. G., Baker, G. R., 1979, Ann. Rev. of Fluid Mech. 11, 95.

Density, $t=0.84t_{cc}$

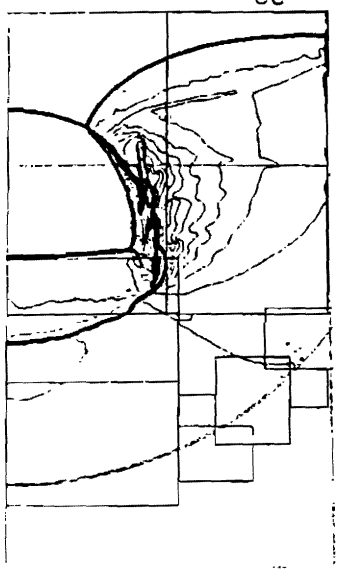

Figure 1

Density, $t=1.05t_{cc}$

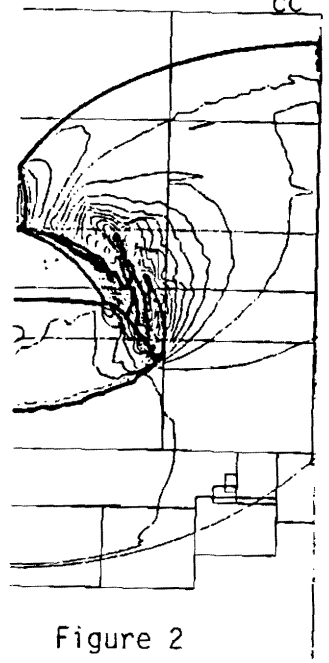

Figure 2

Density, $t=1.26t_{cc}$

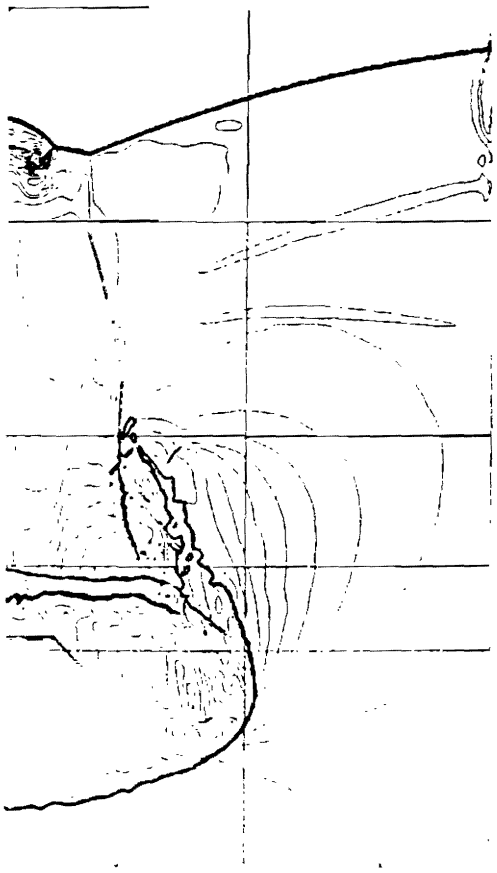

Figure 3

Density, $t=1.68t_{cc}$

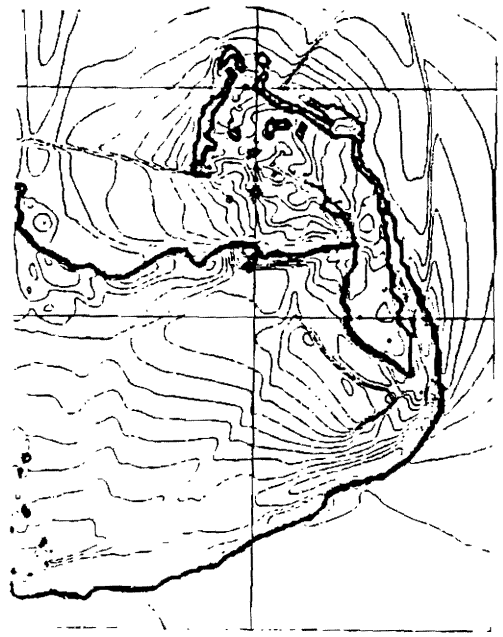

Figure 4

Density, $t=2.1t_{cc}$

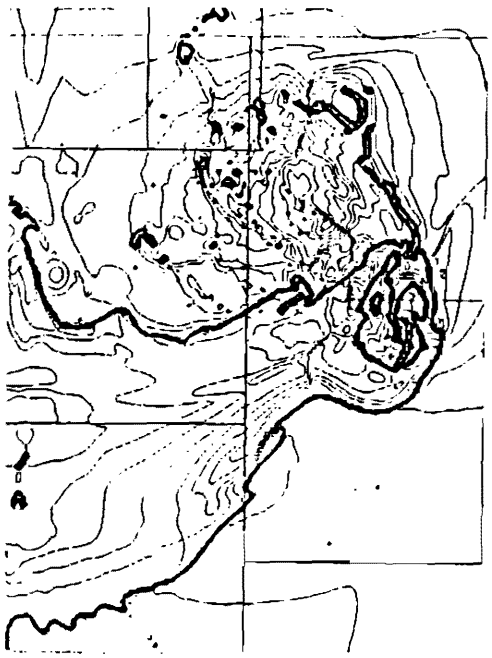

Figure 5

Density, $t=2.5t_{cc}$

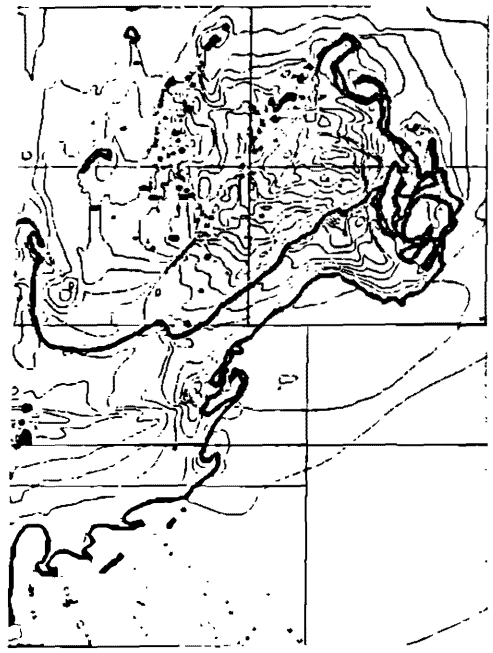

Figure 6

Density, $t=3.78t_{cc}$

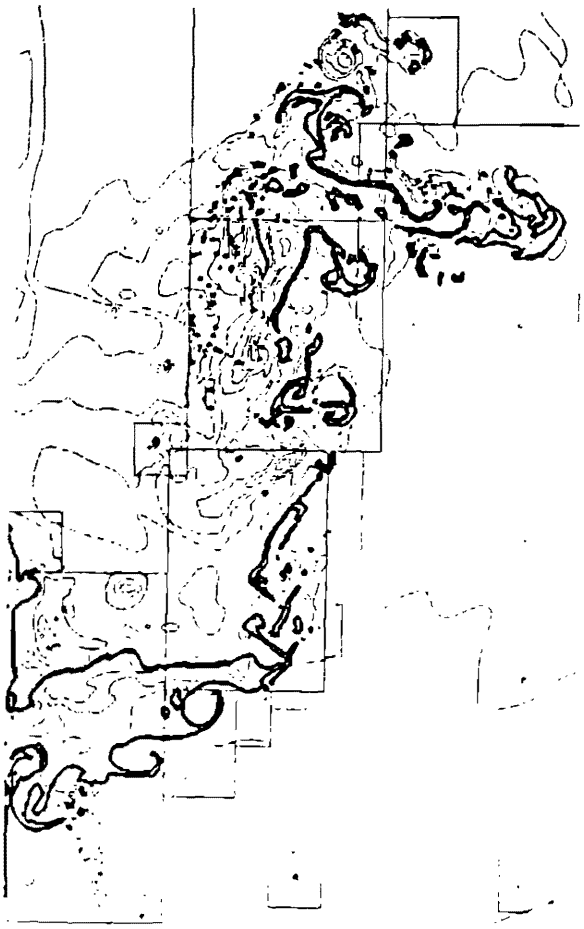

Figure 7

Density, $t=9.7t_{cc}$

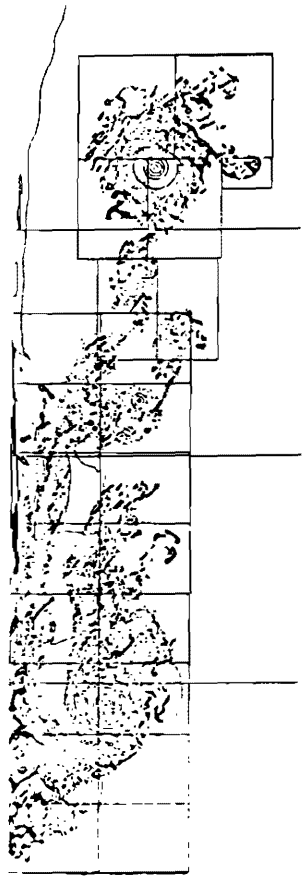

Figure 8

Density, $t=4.2t_{cc}$
$M=10$

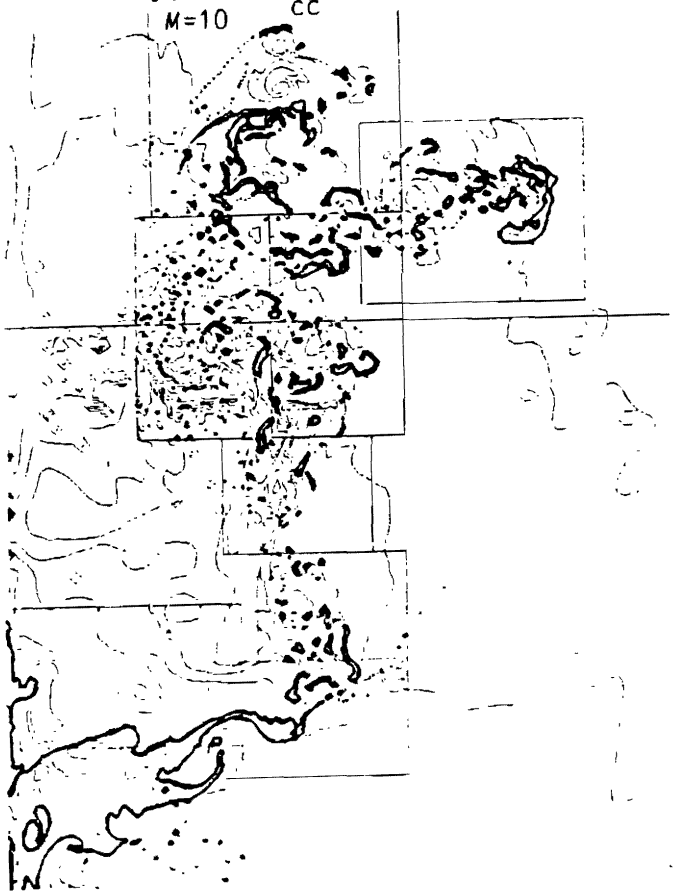

Figure 9a

Density, $t=4.2t_{cc}$
$M=100$

Figure 9b

Vorticity, $t=5.05t_{cc}$

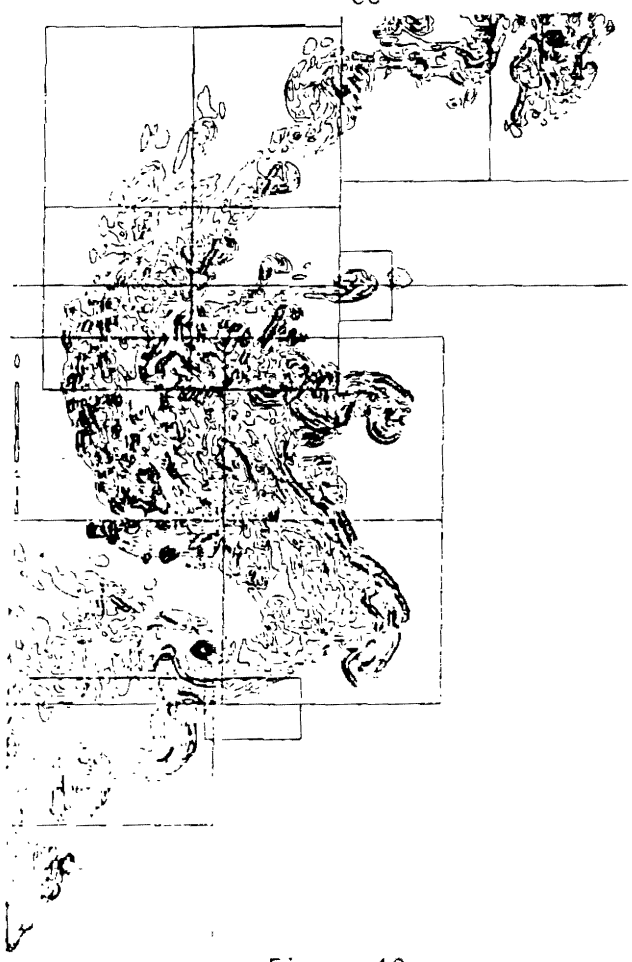

Figure 10